Nanoscale

CORRECTION

View Article Online
View Journal | View Issue

Cite this: *Nanoscale*, 2018, **10**, 20469

Correction: Modelling of thermal transport through a nanocellular polymer foam: toward the generation of a new superinsulating material

Guilong Wang,*[a,b] Chongda Wang,[b] Jinchuan Zhao,[b,c] Guizhen Wang,[d] Chul B. Park,*[b] Guoqun Zhao,*[a] Wouter Van De Walle[e] and Hans Janssen[e]

DOI: 10.1039/c8nr90192a

rsc.li/nanoscale

Correction for 'Modelling of thermal transport through a nanocellular polymer foam: toward the generation of a new superinsulating material' by Guilong Wang *et al.*, *Nanoscale*, 2017, **9**, 5996–6009.

The authors have noticed that the finite discretization for $d\theta_1$ used in calculating the integrals of eqn (34) and (35) in the published paper had significant effects on the calculation accuracy. In the published paper, the range of θ_1 was divided into 1000 equidistant $\Delta\theta_1$ pieces. It was found that the finite discretization was not fine enough, and this led to calculation errors in the cases where the cell wall became extremely thin (<4 nm) either at small cell sizes or at high void fractions. It was found that θ_1 should be divided into several thousands of intervals in discretization to ensure a high calculation accuracy, as shown in Fig. C1.

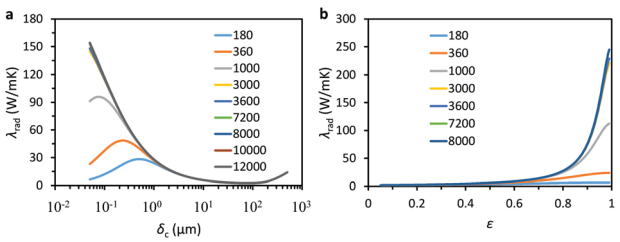

Fig. C1 Calculated correlations between radiative thermal conductivity and (a) cell size at a void fraction of 0.95, and (b) void fraction at a cell size of 50 nm, using different sizes of intervals for numerical discretization.

The authors have recalculated the data presented in the published paper by using a much finer discretization with 10 000 intervals. With a much finer discretization, $\overline{\mathcal{R}_f}$ increased significantly at high void fractions compared to the original case. Subsequently, both λ_{rad} and λ_{eff} decreased obviously at high void fractions. Thus, the originally published Fig. 8 should be replaced by the updated version of Fig. 8 provided below. It should be noted that λ_{con} was not affected by discretization. Thus, the data in Fig. 8b was not changed.

Regarding the data presented in the originally published Fig. 9, λ_{eff}, λ_{rad}, and $\overline{\mathcal{R}_f}$ changed obviously at small cell sizes when using a much finer discretization in the calculations. Thus, this figure should be replaced by the updated version of Fig. 9 provided below. In the updated version of Fig. 9c, it should be noted that the behaviour of the radiative thermal conductivity as a function of the cell size changes significantly in comparison with the data presented in Fig. 9c of the published paper. In the updated version of Fig. 9c, the radiative thermal conductivity reduced first to a certain minimum level, and then increased gradually to a certain maximum value with decreasing cell size. This in turn led to the increase in the total thermal conductivity upon

[a]*Key Laboratory for Liquid-Solid Structural Evolution and Processing of Materials, School of Materials Science and Engineering, Shandong University, Jinan, Shandong 250061, China*
[b]*Microcellular Plastics Manufacturing Laboratory, Department of Mechanical and Industrial Engineering, University of Toronto, Toronto, Ontario M5T3G8, Canada*
[c]*Centre for Precision Engineering, School of Mechatronics Engineering, Harbin Institute of Technology, Harbin, Heilongjiang 150001, China*
[d]*Key Laboratory of Chinese Education Ministry for Tropical Biological Resources, Hainan University, Haikou, Hainan 570228, China*
[e]*KU Leuven, Department of Civil Engineering, Building Physics Section, Kasteelpark Arenberg 40 – Box 2447, BE-3001 Heverlee, Belgium*

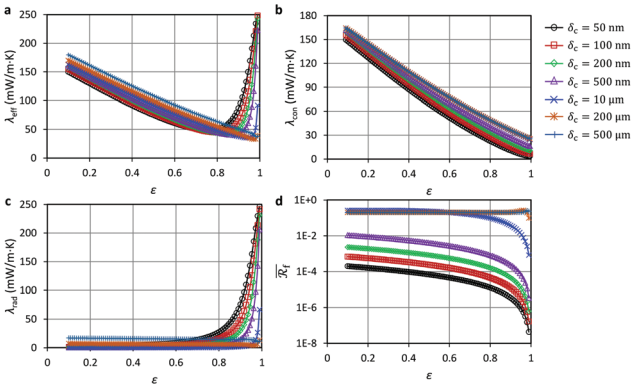

Fig. 8 Dependence of the thermal transport on the foam's void fraction under various cell size levels. (a) Correlation between the void fraction (ε) and the total effective thermal conductivity (λ_{eff}). (b) Correlation between the void fraction and the thermal conductivity contributed by thermal conduction (λ_{con}). (c) Correlation between the void fraction and the radiative thermal conductivity (λ_{rad}). (d) Correlation between the void fraction and the wavelength-averaged reflectance of the single cell wall ($\overline{\mathcal{R}_f}$).

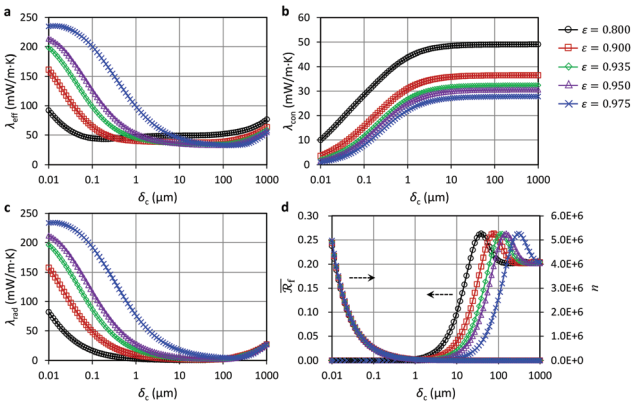

Fig. 9 Dependence of the thermal transport on the foam's cell size under various void fraction levels. (a) Correlation between the cell size (δ_c) and the total effective thermal conductivity (λ_{eff}). (b) Correlation between the cell size and the thermal conductivity contributed by thermal conduction (λ_{con}). (c) Correlation between the cell size and the radiative thermal conductivity (λ_{rad}). (d) Effect of the cell size on the wavelength-averaged reflectance of the single cell wall ($\overline{\mathcal{R}_f}$) and the polymer slab numbers (n).

decreasing the cell size, as shown in the updated version of Fig. 9a, instead of it reaching a certain maximum value and subsequently decreasing with reducing cell size as shown in the original version of Fig. 9a. This phenomenon was due to the sharp decrease in the reflectance of the single cell wall with decreasing cell size (Fig. 9d), and increasing the number of cell walls could not offset the adverse impact on the total reflectance of IR waves.

As shown in the original versions of Fig. 9a and c, both λ_{eff} and λ_{rad} first decreased, then increased, and finally decreased again, upon reducing the cell size. Thus, both λ_{eff} and λ_{rad} showed maximum peak values. In order to explain the final downward trend of the two variables, it was stated in the published paper that the increase in the rate of the cell wall number (n) was much faster than the declining rate of the wavelength-averaged reflectance of the single cell wall ($\overline{\mathcal{R}_f}$). However, this was not true because n and $\overline{\mathcal{R}_f}$ were not compared over an equivalent numerical range. In fact, if an equivalent numerical range were to be employed, it would be found that the decrease in $\overline{\mathcal{R}_f}$ would be so fast that the increase in n could not offset its adverse impact on the total reflectance of IR waves. Subsequently, the maximum peak values that appeared in the original versions of Fig. 9a and c should not have existed, as shown in the updated versions of Fig. 9a and c. It was inferred that, as the cell size reduced indefinitely, $\overline{\mathcal{R}_f}$ would gradually approach zero and $\mathcal{T}_{net}^{unit}$ would approach one. According to eqn (41) shown in the published paper, the radiative thermal conductivity would finally approach its maximum value of $4 \times \sigma_{SB} \times \bar{T}^3 \times L$, which is 257.5 mW m^{-1} K^{-1}.

When calculating with a much finer discretization, $\overline{\mathcal{R}_f}$ decreased significantly at high void fractions compared with the originally published data. Subsequently, both λ_{rad} and λ_{eff} increased significantly at high void fractions in comparison with the orig-

inal data. Thus, Fig. 10 in the published paper should be replaced by the updated version of Fig. 10 provided below. Notably, it can be seen in the updated version of Fig. 10b that the maximum value of λ_{rad} could be up to 250 mW m^{-1} K^{-1}, which is much larger than the maximum value reported in the original version of Fig. 10b. Consequently, the maximum value of λ_{eff} reported in the updated version of Fig. 10a was also much larger than the maximum value reported in the original version of Fig. 10a.

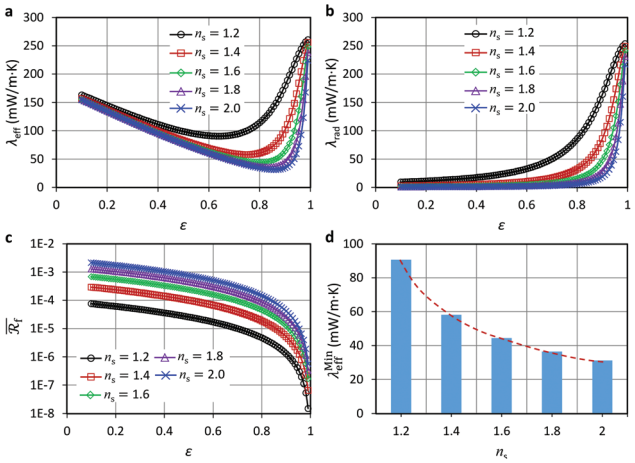

Fig. 10 Effect of the polymer's refractive index on the thermal transport in nanocellular polymer foams (δ_c = 100 nm). (a) Correlation between the void fraction and the total effective thermal conductivity. (b) Correlation between the void fraction and the radiative thermal conductivity. (c) Correlation between the void fraction and the wave-averaged reflectance of the single cell wall. (d) Dependence of the minimum total effective thermal conductivity of the nanocellular foam (δ_c = 100 nm) on the refractive index.

For the same reason, Fig. 11 in the published paper should also be replaced by the updated version of Fig. 11 provided below. Notably, both λ_{rad} and λ_{eff} increased significantly at high void fractions in comparison with the original data. However, the change in discretization here did not change the variation trend of the variables. Moreover, the minimum effective thermal conductivity (λ_{eff}^{Min}) calculated for the different cases only changed slightly.

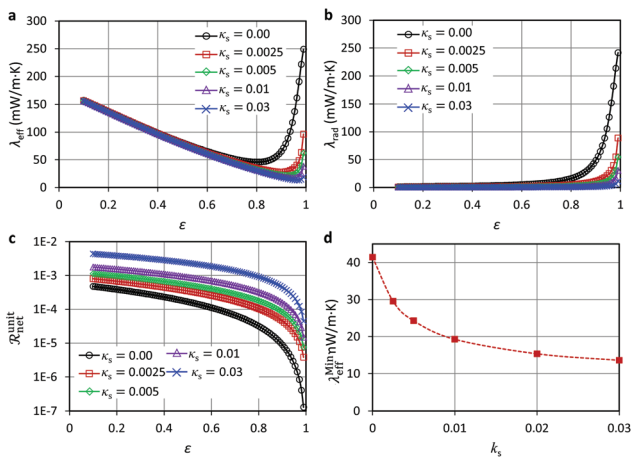

Fig. 11 Effect of the polymer's absorption index on the thermal transport in the nanocellular foams (δ_c = 100 nm). (a) Correlation between the void fraction and the total effective thermal conductivity. (b) Correlation between the void fraction and the radiative thermal conductivity. (c) Correlation between the void fraction and the net fraction of the radiation energy reflected by the basic three-slab unit. (d) Dependence of the minimum total effective thermal conductivity of the nanocellular foam (δ_c = 100 nm) on the absorption index.

Fig. 12 in the published paper should also be replaced by the updated version of Fig. 12 provided below. Overall, the contour isotherms of the thermal conductivity did not exhibit any obvious changes in comparison with the original version of Fig. 12, except for the data at small cell sizes and high void fractions.

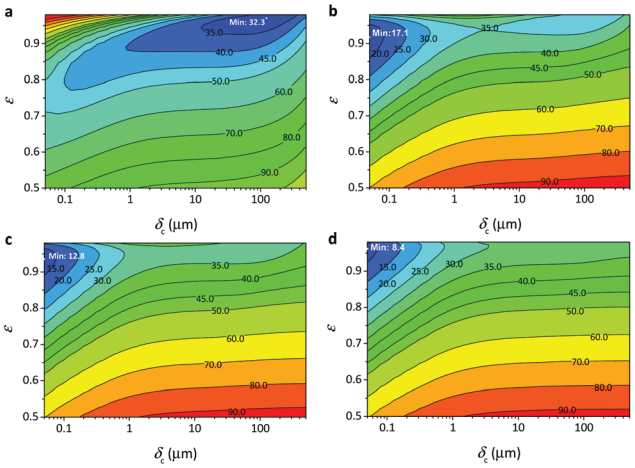

Fig. 12 The calculated colour contour isotherms of the thermal conductivity as a function of the cell size and the void fraction under various absorption coefficients. (a) κ = 0.000. (b) κ = 0.005. (c) κ = 0.010. (d) κ = 0.030.

Also, the formulas (23)–(33) in the paper need to be corrected because the refraction angle, θ_2, which should be a complex number, was mistakenly processed as a real number when preparing the original article. However, these errors did not affect the calculation results, because θ_2 had been correctly taken as a complex number in all previous modelling and calculation works.

The formula (23) in the article should be changed to the following:

$$\begin{cases} \mathcal{R}_f = \dfrac{\rho_{gs}^2 e^{4\pi\delta_w \upsilon_s/\lambda} + \rho_{sg}^2 e^{-4\pi\delta_w \upsilon_s/\lambda} + 2\rho_{gs}\rho_{sg}\cos\omega_1}{e^{4\pi\delta_w \upsilon_s/\lambda} + \rho_{gs}^2\rho_{sg}^2 e^{-4\pi\delta_w \upsilon_s/\lambda} + 2\rho_{gs}\rho_{sg}\cos\omega_2} \\ \omega_1 = \phi_{sg} - \phi_{gs} + 4\pi\delta_w u_s/\lambda \\ \omega_2 = \phi_{gs} + \phi_{sg} + 4\pi\delta_w u_s/\lambda \end{cases} \tag{23}$$

In the updated formula (23), u_s and υ_s are employed to simplify the notation, and their values are determined by $u_s + i\upsilon_s = (n_s + i\kappa_s)\cos\theta_2$. To calculate the complex refraction angle, θ_2, the formula (24) should be changed to:

$$\theta_2 = \sin^{-1}\left(n_g \frac{\sin\theta_1}{n_s + i\kappa_s}\right) \tag{24}$$

Accordingly, for the incident radiation wave with the electric vector perpendicular to the plane of incidence, formulas (25) and (26) which were used to determine ρ_{gs}, ρ_{sg}, ϕ_{gs}, and ϕ_{sg} should be respectively replaced with the following formulas:

$$\rho_{sg} = -\rho_{gs} = \sqrt{\frac{(n_g\cos\theta_1 - u_s)^2 + \upsilon_s^2}{(n_g\cos\theta_1 + u_s)^2 + \upsilon_s^2}} \tag{25}$$

$$\phi_{sg} = \phi_{gs} = \tan^{-1}\left(\frac{2n_g\upsilon_s\cos\theta_1}{u_s^2 + \upsilon_s^2 - n_g^2\cos^2\theta_1}\right) \tag{26}$$

Meanwhile, for the incident radiation wave with the electric vector parallel to the plane of incidence, formulas (27) and (28) should be respectively changed to the following:

$$\rho_{sg} = -\rho_{gs} = \sqrt{\frac{\left[(n_s^2 - \kappa_s^2)\cos\theta_1 - n_g u_s\right]^2 + (2n_s\kappa_s\cos\theta_1 - n_g\upsilon_s)^2}{\left[(n_s^2 - \kappa_s^2)\cos\theta_1 + n_g u_s\right]^2 + (2n_s\kappa_s\cos\theta_1 + n_g\upsilon_s)^2}} \tag{27}$$

$$\phi_{sg} = \phi_{gs} = \tan^{-1}\left(\frac{2n_g\cos\theta_1[2n_s\kappa_s u_s - (n_s^2 - \kappa_s^2)\upsilon_s]}{(n_s^2 + \kappa_s^2)^2\cos^2\theta_1 - n_g^2(u_s^2 + \upsilon_s^2)}\right) \tag{28}$$

The formula (29) used to calculate the transmittance of polymer film in the article should be changed to the following:

$$\mathcal{T}_f = \frac{\tau_{gs}^2\tau_{sg}^2 e^{-4\pi\delta_w\upsilon_s/\lambda}}{1 + \rho_{gs}^2\rho_{sg}^2 e^{-8\pi\delta_w\upsilon_s/\lambda} + 2\rho_{gs}\rho_{sg}e^{-4\pi\delta_w\upsilon_s/\lambda}\cos\omega_2} \tag{29}$$

For the incident radiation wave with the electric vector perpendicular to the plane of incidence, formulas (30) and (31) used to determine τ_{gs} and τ_{sg} should be respectively replaced with the following formulas:

$$\tau_{gs} = \frac{2n_g \cos\theta_1}{\sqrt{(n_g \cos\theta_1 + u_s)^2 + v_s^2}} \tag{30}$$

$$\tau_{sg} = \frac{2\sqrt{u_s^2 + v_s^2}}{\sqrt{(n_g \cos\theta_1 + u_s)^2 + v_s^2}} \tag{31}$$

Meanwhile, for the incident radiation wave with the electric vector parallel to the plane of incidence, formulas (32) and (33) should be respectively changed to the following:

$$\tau_{gs} = \frac{2(n_s^2 + \kappa_s^2)\cos\theta_1}{\sqrt{[(n_s^2 - \kappa_s^2)\cos\theta_1 + n_g u_s]^2 + (2n_s\kappa_s \cos\theta_1 + n_g v_s)^2}} \tag{32}$$

$$\tau_{sg} = \frac{2n_g\sqrt{u_s^2 + v_s^2}}{\sqrt{[(n_s^2 - \kappa_s^2)\cos\theta_1 + n_g u_s]^2 + (2n_s\kappa_s \cos\theta_1 + n_g v_s)^2}} \tag{33}$$

In addition to the above corrections, eqn (36) in the published paper should be changed to the following:

$$f(\lambda) = \frac{2c^2\pi h}{\lambda^5 \exp(hc/\lambda k_B T)} \tag{36}$$

These errors do not affect the main conclusions of the paper. The Royal Society of Chemistry apologises for these errors and any consequent inconvenience to authors and readers.